Electronic supplementary information (ESI)

SDS-induced multi-stage unfolding of a small globular protein through different denatured states revealed by single-molecule fluorescence

Georg Krainer,*‡§[a] Andreas Hartmann,[a‡] Vadim Bogatyr,[a‡$] Janni Nielsen,[c] Michael Schlierf*[a,b] and Daniel E. Otzen*[c]

[a] B CUBE – Center for Molecular Bioengineering, TU Dresden, Tatzberg 41, 01307 Dresden, Germany. E-Mail: georg.krainer@tu-dresden.de, michael.schlierf@tu-dresden.de

[b] Cluster of Excellence Physics of Life, TU Dresden, 01062 Dresden, Germany.

[c] Interdisciplinary Nanoscience Center (iNANO), Aarhus University, Gustav Wieds Vej 14, 8000 Aarhus, Denmark. E-mail: dao@inano.au.dk

* Corresponding authors.

‡ These authors contributed equally to this work.

§ Present address: Centre for Misfolding Diseases, Department of Chemistry, University of Cambridge, Lensfield Road, CB2 1EW Cambridge, UK. E-mail: gk422@cam.ac.uk

$ Present address: Department of Physics and Astronomy, LaserLaB Amsterdam, Vrije Universiteit Amsterdam, De Boelelaan 1081, 1081 HV Amsterdam, Netherlands.

Supplementary Figures

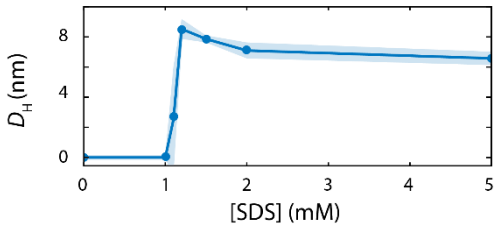

Figure S1. CMC determination for SDS in 50 mM TRIS, 150 mM NaCl, pH 7.4 and at 25°C. Shown is the average hydrodynamic diameter (D_H) as a function of SDS concentration as determined by DLS. The CMC of SDS was determined to be 1.1 mM.

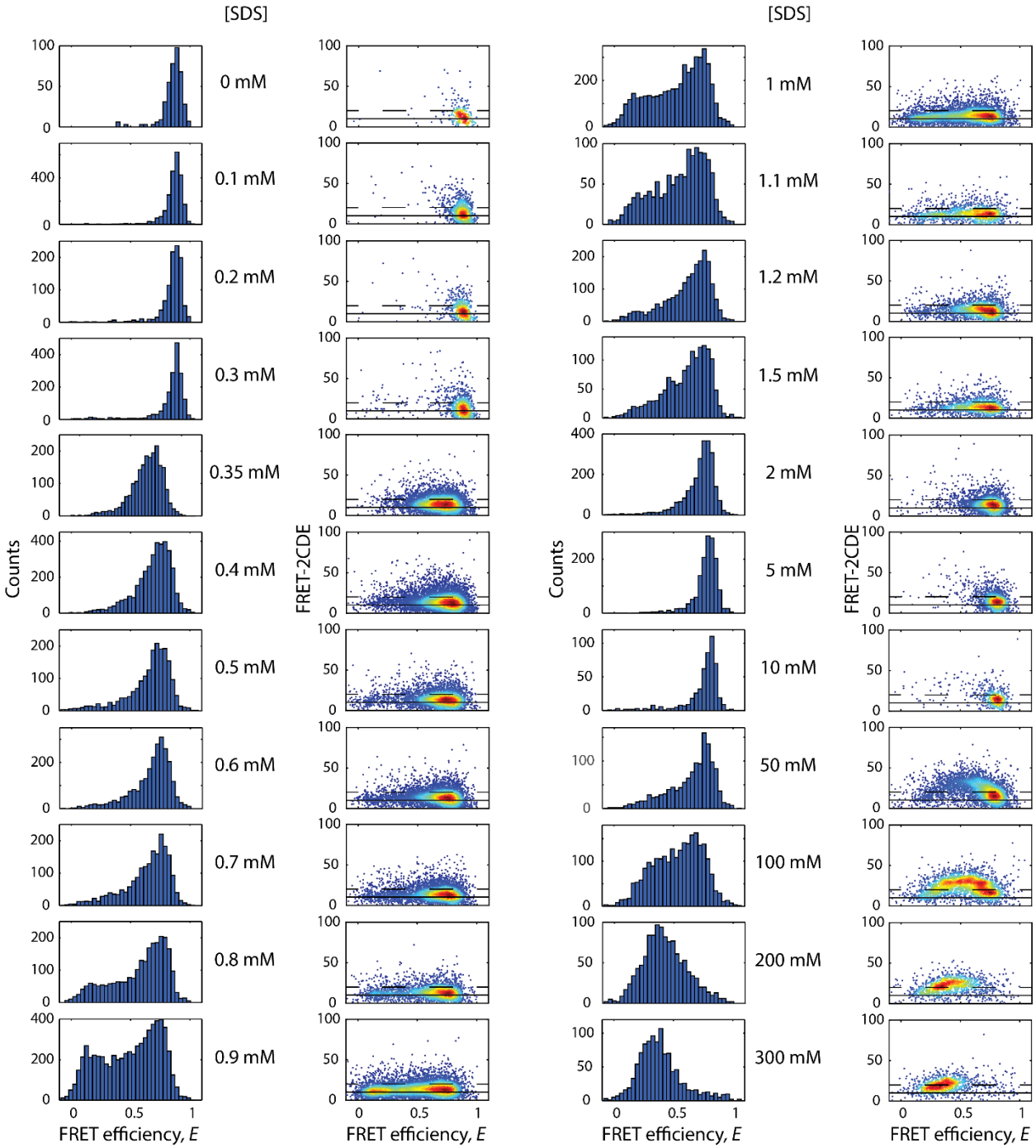

Figure S2. Denaturation series of S6 in SDS. FRET efficiency histograms and the corresponding FRET-2CDE plots of S6 at increasing SDS concentration (0–300 mM).

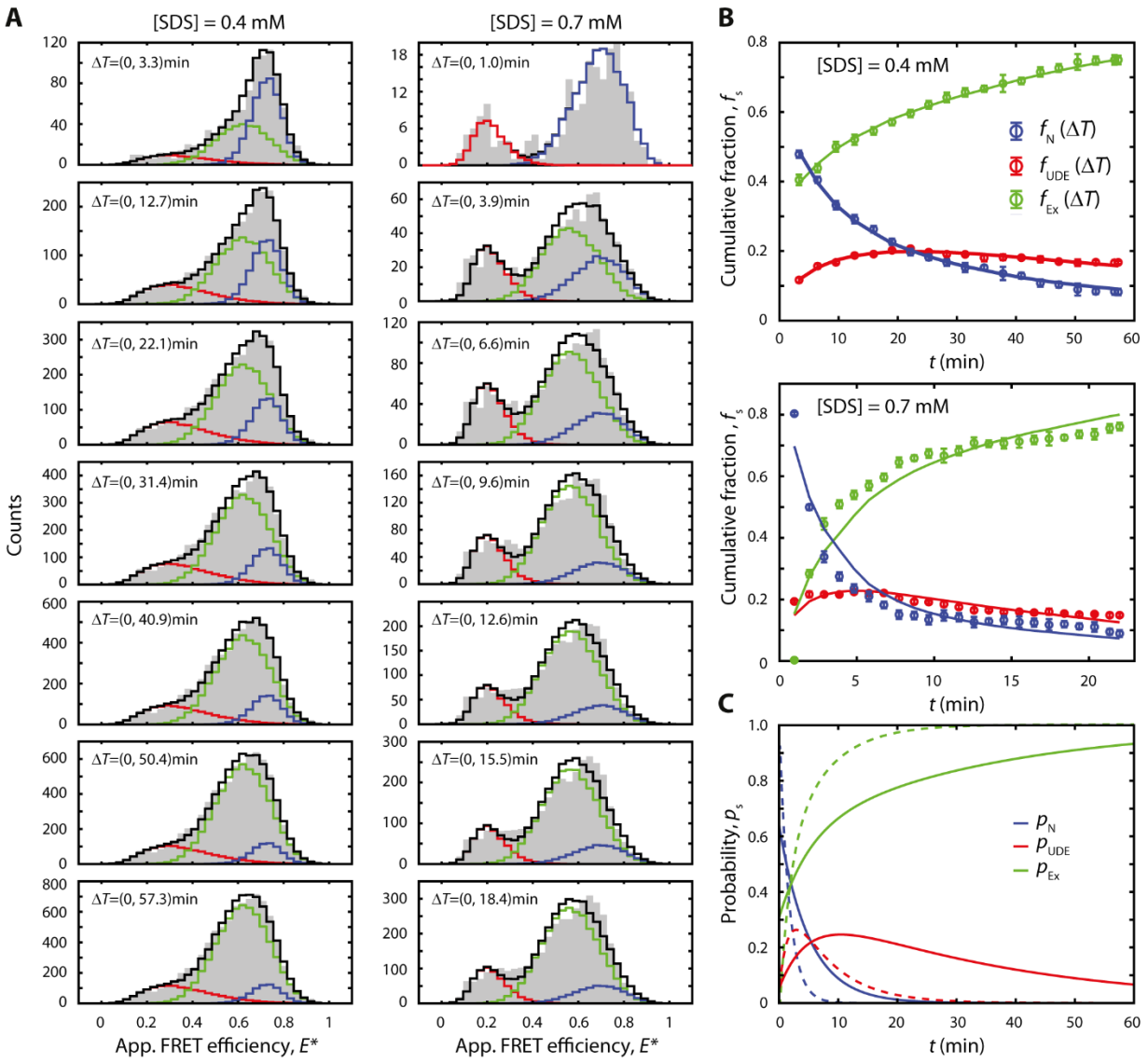

Figure S3. Slow unfolding dynamics of S6 at 0.4 mM and 0.7 mM SDS quantified by PDA. (A) Time series of apparent FRET efficiency histograms (grey) collected from increasing time intervals Δ*T* at 0.4 mM SDS (left column) and 0.7 mM SDS (right column). The blue, green, and red cityscapes describe the native N, expanded Ex and unfolded/denatured ensemble UDE subpopulations derived from three-state static PDA fits, respectively. **(B)** Resulting cumulative fractions, f_s, of the three-state static PDA. The solid lines represent the fitting results of the kinetic analysis (described in Supplementary Methods) yielding interconversion rates of $k_{N\rightarrow UDE} = (0.09 \pm 0.006)$ min^{-1}, $k_{UDE\rightarrow Ex} = (0.030 \pm 0.002)$ min^{-1} and $k_{N\rightarrow Ex} = (0.108 \pm 0.007)$ min^{-1} for 0.4 mM SDS and $k_{N\rightarrow UDE} = (0.22 \pm 0.07)$ min^{-1}, $k_{UDE\rightarrow Ex} = (0.15 \pm 0.04)$ min^{-1} and $k_{N\rightarrow Ex} = (0.39 \pm 0.07)$ min^{-1} for 0.7 mM SDS. **(C)** Corresponding probability functions (Eq. 2) using the kinetic results of panel B for 0.4 mM SDS (solid lines) and 0.7 mM SDS (dashed lines).

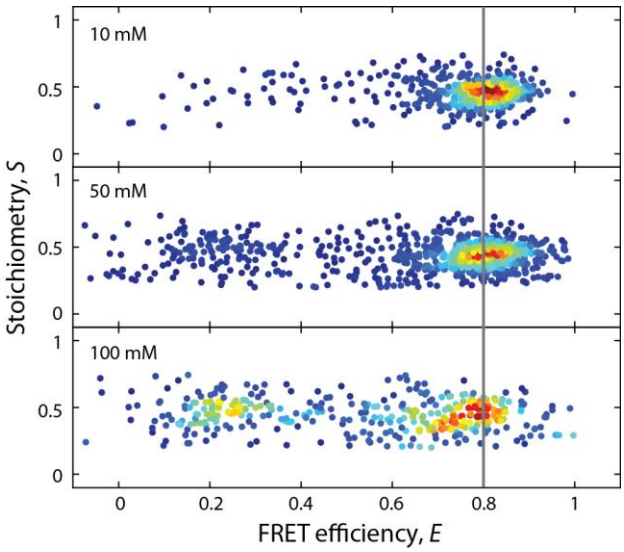

Figure S4. Filtered stoichiometry vs. FRET efficiency plot at different SDS concentrations. The upper panel shows stoichiometry vs. FRET efficiency at 10 mM SDS (without FRET-2CDE filtering). The scatter plots at 50 and 100 mM SDS (middle and lower panel, respectively) show molecules with FRET-2CDE < 12 (static FRET molecules). The grey solid line represents the centre position of the compact state distribution at E_C = 0.80.

Supplementary Table

Table S1: Fluorescence lifetimes and time-resolved anisotropies at different SDS concentrations. The fluorescence lifetime in the absence of the acceptor, $\tau_{D(0)}$, shows no significant change for increasing SDS concentrations. This implies a constant quantum yield of the donor fluorophore. Because the rotational correlation times of the donor and acceptor, $\rho_{GG,fast}$ and $\rho_{RR,fast}$, are smaller than the minimal time of energy transfer, $1/k_{FRET}$, and because the combined anisotropy, r_C, is smaller than 0.2, a sufficient rotational averaging of the dipoles ($\kappa^2 = 2/3$) can be assumed at 0.6 and 10 mM [SDS]. In the case of 0.2 mM [SDS], the rotational correlation time of the donor is one order of magnitude faster than the minimal time of energy transfer indicating as well a sufficient rotational averaging.

high FRET

[SDS] (mM)	$\tau_{D(0)}$ (ns)	$\tau_{D(A)}$ (ns)	$(1/k_{FRET})$ (ns)	$\rho_{GG,fast}$ (ns)	$\rho_{RR,fast}$ (ns)
0.2	3.40 ± 0.01	0.92 ± 0.04	1.27 ± 0.08	0.15 ± 0.09	1.78 ± 1.20
0.6	3.43 ± 0.01	1.46 ± 0.02	2.54 ± 0.06	0.18 ± 0.03	1.74 ± 0.45
10	3.45 ± 0.02	1.32 ± 0.02	2.14 ± 0.05	0.29 ± 0.10	0.88 ± 0.48

[SDS] (mM)	$r_{\infty,GG}$	$r_{\infty,GR}$	$r_{\infty,RR}$	r_C
0.2	0.10 ± 0.03	0.044 ± 0.004	0.13 ± 0.06	0.11 ± 0.03
0.6	0.149 ± 0.009	0.046 ± 0.001	0.17 ± 0.02	0.16 ± 0.01
10	0.11 ± 0.02	0.039 ± 0.003	0.19 ± 0.02	0.14 ± 0.02

Supplementary Methods

Quantification of millisecond interconversion dynamics between the denatured state D and the compact state C by dynamic probability distribution analysis (dPDA).

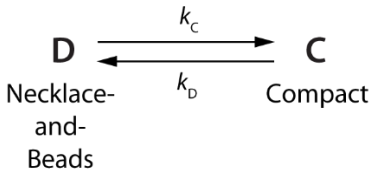

Scheme S1: Two-state model describing the interconversion dynamics between the denatured state D and the compact state C of S6 at hundreds of millimolar [SDS].

Millisecond interconversion dynamics between the denatured state D and the compact state C (Scheme S1) were quantified by dynamic two-state probability distribution analysis (dPDA). Briefly, dPDA remodels the shape of the apparent FRET efficiency histograms using a Monte Carlo simulation-based approach to retrieve FRET states and their interconversion rate constants. We used a dPDA method that incorporates Gaussian distance distributions for the two FRET states that account for additional widths in excess of shot-noise broadening. The fitting parameters used in the dPDA fit were the apparent FRET efficiencies of the denatured and compact states, E_D and E_C, the corresponding interconversion rates, k_D and k_C, and the width of the underlying distance distributions of the denatured and compact states, σ_D and σ_C, respectively. The optimisation of the dPDA fit is performed by minimisation of the reduced chi-square. Further details on the analysis method were described earlier.[1,2]

Quantification of minute timescale interconversion dynamics between the native state N, the expanded state Ex, and the unfolded/denatured ensemble UDE by slow dynamic PDA.

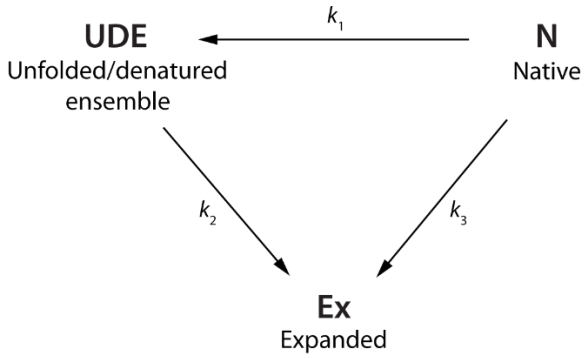

Scheme S2: Three-state model describing the interconversion dynamics between the native state N, the expanded state Ex, and the unfolded/denatured ensemble UDE of S6 at SDS concentrations in the range of 0.4–1.5 mM. The reduced model comprises only the three major transitions k_1 (*i.e.*, $k_{N\rightarrow UDE}$), k_2 (*i.e.*, $k_{UDE\rightarrow Ex}$) and k_3 (*i.e.*, $k_{N\rightarrow Ex}$), which fully describes the relaxation kinetics and equilibrium state of S6 at low SDS concentrations.

The reaction kinetics depicted in Scheme S2 are described by the following system of ordinary differential equations (ODE):

$$\begin{aligned} \frac{d[\mathrm{N}]}{dt} &= -(k_1+k_3)[\mathrm{N}] \\ \frac{d[\mathrm{UDE}]}{dt} &= k_1[\mathrm{N}] - k_2[\mathrm{UDE}] \\ \frac{d[\mathrm{Ex}]}{dt} &= k_2[\mathrm{UDE}] + k_3[\mathrm{N}] \end{aligned} \qquad (1)$$

here [N], [Ex] and [UDE] are the concentrations of the protein in the native N, expanded Ex, and unfolded/denatured ensemble UDE states, respectively. Solving the system of ODEs in Eq. 1 we obtain:

$$\begin{aligned} p_N(t) &= p_N(0)\exp(-(k_1+k_3)t) \\ p_{Ex}(t) &= 1-\lambda_1\exp(-k_2t)-\lambda_2\exp(-(k_2+k_3)t) \\ p_{UDE}(t) &= \lambda_1\exp(-k_2t)-\lambda_3\exp(-(k_1+k_3)t) \end{aligned} \qquad (2)$$

$$\lambda_1 = \frac{p_N(0) \cdot k_1 + p_{UDE}(0) \cdot (k_1 + k_3 - k_2)}{(k_1 + k_3 - k_2)}$$

$$\lambda_2 = \frac{p_N(0) \cdot (k_3 - k_2)}{(k_1 + k_3 - k_2)}$$

$$\lambda_3 = \frac{p_N(0) \cdot k_1}{(k_1 + k_3 - k_2)}$$

where $p_N(0)$, $p_{Ex}(0)$ and $p_{UDE}(0)$ denote the initial probability of the N, Ex, and UDE states at $t = 0$, respectively.

Slow dynamic PDA. In order to quantify the kinetic rates of the slow conformational changes of S6 as depicted in Scheme S2, first the state-related apparent FRET efficiencies had to be derived from the measured histograms by static PDA. For this purpose, the overall shape of the experimental apparent FRET efficiency histogram (FEH) was fitted to a theoretical FEH using Monte Carlo simulations assuming a three-state model. The three-state model comprised the apparent FRET efficiencies E_N, E_{Ex}, and E_{UDE} corresponding to the N, Ex, and UDE states, respectively. To account for additional widths in excess of shot-noise broadening, individual distances, $R_{N,Ex,UDE}$, were drawn for each burst (corresponding to either the N, Ex, and UDE states, respectively) from a Gaussian distribution with $\sigma_{N,Ex,UDE}$ describing the given width of the distributions, respectively. During chi-square optimization for every set of parameters {E_N, σ_N, E_{Ex}, σ_{Ex}, E_{UDE}, σ_{UDE}, p_N, p_{Ex}} a theoretical FRET efficiency histogram was generated by drawing the number of molecules in the N, Ex, and UDE states, n_N, n_{Ex} and n_{UDE}, respectively, from a multinomial distribution. Subsequently, the number of acceptor photons, $a_{N,Ex,UDE}$, were drawn from the binomial distribution:

$$P(a_s|f_s, E_s) = \binom{f_s}{a_s} {E_s}^{a_s} (1 - E_s)^{f_s - a_s} \quad (3)$$

where *s* refers to the molecular state {N, Ex, UDE}. The apparent FRET efficiency histogram of each optimization step was then collected from the ratios $a_{N,Ex,UDE}/F$ of all randomized molecules and averaged by the oversampling factor *K*. The static PDA fit, yielded $E_N = 0.723 \pm 0.004$, $E_{Ex} = 0.619 \pm 0.010$, $E_{UDE} = 0.337 \pm 0.036$, $\sigma_N = (0.20 \pm 0.02)$ nm, $\sigma_{Ex} = (0.39 \pm 0.02)$ nm and $\sigma_{UDE} = (0.67 \pm 0.12)$ nm for 0.4 mM SDS and $E_N = 0.690 \pm 0.003$, $E_{Ex} = 0.564 \pm 0.003$, $E_{UDE} = 0.210 \pm 0.005$, $\sigma_N = (0.38 \pm 0.01)$ nm, $\sigma_{Ex} = (0.41 \pm 0.01)$ nm and $\sigma_{UDE} = (0.41 \pm 0.03)$ nm for 0.7 mM SDS.

In a next step, the obtained burst data at the respective [SDS] concentrations were analysed. Due to the limited number of transitions, cumulative histograms were built of molecules occurring in a

certain time interval $\Delta T = (0, i \cdot \Delta t)$ with Δt = 200 s for 0.4 mM SDS and Δt = 60 s for 0.7 mM SDS. The fraction of molecules in the N, Ex, and UDE states, f_s, of each time interval was then derived from a static three-state PDA fit by using the E_s and σ_s from the first analysis. Figure S3A shows an excerpt of the resulting PDA fits for increasing time intervals, where the blue, green and red cityscapes correspond to the number of molecules in the subpopulations of the N, Ex, and UDE states, respectively.

Finally, the kinetic rates of S6 were derived by applying Eq. 4 to the extracted cumulative fractions, f_s (Figure S3B). To avoid time binning, advantage was taken of the individual burst arrival times:

$$f_s(t) = \sum_{t_i<t} p_s(t_i)/N_{t_i<t} \tag{4}$$

here t_i denotes the arrival time of the i-th burst, $p_s(t)$ the probability function of state s (Eq. 2) and $N_{t_i<t}$ the number of bursts with arrival times smaller than t. The global fit of all three fractions (Figure S3B, solid lines) revealed interconversion rates of k_1 = (0.090 ± 0.006) min^{-1}, k_2 = (0.030 ± 0.002) min^{-1} and k_3 = (0.108 ± 0.007) min^{-1} for 0.4 mM SDS and k_1 = (0.22 ± 0.07) min^{-1}, k_2 = (0.15 ± 0.04) min^{-1} and k_3 = (0.39 ± 0.07) min^{-1} for 0.7 mM SDS (note: $k_1 = k_{N\rightarrow UDE}$, $k_2 = k_{UDE\rightarrow Ex}$, and $k_3 = k_{N\rightarrow Ex}$; see Scheme S2). The resulting probability functions $p_s(t)$ are shown in Figure S3C.

Supplementary References

1 A. Hartmann, G. Krainer, S. Keller and M. Schlierf, *Anal. Chem.*, 2015, **87**, 11224–11232.

2 G. Krainer, A. Hartmann, A. Anandamurugan, P. Gracia, S. Keller and M. Schlierf, *J. Mol. Biol.*, 2018, **430**, 554–564.